RSC Advances

PAPER

View Article Online
View Journal | View Issue

Cite this: *RSC Adv.*, 2020, **10**, 15677

A hybrid lipid membrane coating "shape-locks" silver nanoparticles to prevent surface oxidation and silver ion dissolution†

Thomas J. Miesen, Arek M. Engstrom, Dane C. Frost, Ramya Ajjarapu, Rohan Ajjarapu, Citlali Nieves Lira and Marilyn R. Mackiewicz *

The controlled synthesis of stable silver nanoparticles (AgNPs), that do not undergo surface oxidation and Ag^+ ion dissolution, continues to be a major challenge. Here the synthesis of robust hybrid lipid-coated AgNPs, comprised of L-α-phosphatidylcholine (PC) membranes anchored by a stoichiometric amount of long-chained hydrophobic thiols and sodium oleate (SOA) as hydrophobic binding partners, that do not undergo surface oxidation and Ag^+ ion dissolution, is described. UV-Visible (UV-Vis) spectroscopy, transmission electron microscopy (TEM), and inductively coupled plasma mass spectrometry (ICP-MS) demonstrate that in the presence of strong oxidants, such as potassium cyanide (KCN), the hybrid lipid-coated AgNPs are stable and do not undergo surface oxidation even in the presence of membrane destabilizing surfactants. UV-Vis studies show that the stability of hybrid lipid-coated AgNPs of various sizes and shapes is dependent on the length of the thiol hydrocarbon chain and can be ranked in the order of increasing stability as follows: propanethiol (PT) < hexanethiol (HT) ≤ decanethiol (DT). UV-Vis and ICP-MS studies show that the hybrid lipid-coated AgNPs do not change in size or shape confirming that the AgNPs do not undergo surface oxidation and Ag^+ ion dissolution when placed in the presence of strong oxidants, chlorides, thiols, and low pH. Long-term stability studies, over 21 days, show that the hybrid lipid-coated AgNPs do not release Ag^+ ions and are more stable. Overall, these studies demonstrate hybrid membrane encapsulation of nanomaterials is a viable method for stabilizing AgNPs in a "shape-locked" form that is unable to undergo surface oxidation, Ag^+ ion release, aging, or shape conversion. More importantly, this design strategy is a simple approach to the synthesis and stabilization of AgNPs for a variety of biomedical and commercial applications where Ag^+ ion release and toxicity is a concern. With robust and shielded AgNPs, investigators can now evaluate and correlate how the physical features of AgNPs influence toxicity without the confounding factor of Ag^+ ions present in samples. This design strategy also provides an opportunity where the membrane composition can be tuned to control the release rate of Ag^+ ions for optimizing antimicrobial activity.

Received 23rd February 2020
Accepted 14th April 2020

DOI: 10.1039/d0ra01727b

rsc.li/rsc-advances

Introduction

Engineered nanomaterials are used for a wide range of applications in many different fields and are a rapidly growing technology.[1–3] Every year about 500 tons of silver nanoparticles (AgNPs) are produced for many industrial and biomedical applications because of their unique optical, chemical, physical, biological, catalytic, and broad-spectrum antimicrobial activity.[4–15] Harnessing their antimicrobial power, AgNPs are incorporated into food packaging,[1–3] clothing,[16–18] and in medical products such as wound gels,[19,20] bandages,[21–23] coatings on medical catheters,[24,25] and cardiovascular implants.[15,26,27] In addition, AgNPs are utilized in various subfields of medicine as plasmonic antennas, diagnostic agents, and as nanoprobes to target and image small molecules such as DNA, proteins, cell tissue, and tumors.[28–30] Because AgNPs exhibit a red-shift in the plasmonic extinction band in the near-infrared (NIR) optical window region (700–900 nm), they are also used as imaging and photothermal agents to visualize and destroy cancer cells.[31,32] Their wide applicability and versatility have led to an increased demand for optimized AgNPs with tuned physical, optical, and chemical properties for various applications. More importantly, biocompatible and stable AgNPs with minimal impact on human health and the environment are of significant interest.

It is well-known that the physical, optical, and catalytic properties of AgNPs are strongly influenced by their size, shape,

Department of Chemistry, Portland State University, Portland, OR 97207, USA. E-mail: mackiewi@pdx.edu

† Electronic supplementary information (ESI) available: Images of AgNPs at various time points in the presence of 50 mM NaCl, UV-Vis spectra showing a change in the LSPR band under a variety of conditions, the procedure for estimating nanoparticle and lipid concentrations, and TEM histograms showing size and shape distributions. See DOI: 10.1039/d0ra01727b

and surface properties and can be optimized using various synthetic methods, reducing agents, and stabilizers.[33–37] Synthetic methods for AgNP synthesis include physical methods, such as evaporation–condensation techniques[38,39] or laser ablation,[40] and chemical methods where metal salts are reduced in the presence of capping agents.[41–45] Depending on the capping agent used in chemical synthesis, AgNPs can be dispersed in aqueous or organic solvents and stabilized to minimize aggregation either by steric or electrostatic repulsion. Ligands used as capping agents include citrate, halides, carboxylates, amines, and polyoxoanions that produce AgNPs with anionic or cationic charge, while polymers such as poly *N*-vinyl-2-pyrrolidone (PVP), polyethylene glycol (PEG), polymethacrylic acid (PMAA), polymethylmethacrylate (PMMA) and dodecanethiol allow for steric repulsion to prevent AgNP aggregation.[42,46] Chemical methods also allow for a wide variety of reducing agents such as glucose, hydrazine, ascorbate, ethylene glycol, citrate, dimethylformamide, dextrose, and sodium borohydride ($NaBH_4$) to control the rate of reduction and formation of AgNPs of various size and shapes.[47,48] Although these synthetic methods have produced AgNPs shaped as spheres,[49] cubes,[50] bipyramids,[51] stars,[52] nanoprisms,[53] triangular plates[53] these methods are energy-intensive, the size and shape distributions are not always homogenous, and chemicals used can be toxic. Consequently, this has given rise to alternative green synthetic approaches employing biological entities such as microorganisms[10,12,54,55] and plant extracts[4,56–63] to replace more complex syntheses of AgNPs free from toxic capping agents and hazardous byproducts.

While these synthetic strategies tune specific physical, optical, and chemical properties, other critical parameters remained largely unexplored. For example, there are very few methods that focus on control of surface oxidation, Ag^+ ion dissolution, and AgNP shape conversion in both biological and environmental media conditions. Consequently, the inability to control these critical parameters limits the long-term stability, shelf-life and use of AgNPs in commercial and biomedical applications where nanomaterial degradation, Ag^+ ion release, and toxicity is a challenge and concern. For instance, in antibacterial applications, the controlled release of Ag^+ ions is a highly desirable property of AgNPs for optimal antimicrobial activity in addition to size, shape, surface charge, concentration, and colloidal state.[51–54] However, there are applications where the presence of Ag^+ ions is not always desirable. For example, toxicology studies with AgNPs have shown associated cytotoxicity, genotoxicity, and inflammatory response in plants,[64] zebrafish embryos,[65] and mammalian cell culture models,[66–69] thereby raising concerns about the potential environmental and human health risks of AgNPs. In these studies, Ag^+ ions are always present and is a confounding factor making it difficult to interpret data and elucidate how the physicochemical features, shape, size, surface chemistry, and surface area of AgNPs influence toxicity. That is when surface oxidation and Ag^+ ion dissolution lead to changes in shape and size it is difficult to effectively assess how size or shape influences toxicity. Toxicology studies are limited by the lack of well-controlled and stable AgNP batches of varying size, shape, surface area, and charge without Ag^+ ions. Accordingly, there is a great need for alternative design approaches for the synthesis of well-defined AgNPs without Ag^+ to assess the fate, biouptake, and ecotoxicity of AgNPs.

Other applications where the presence of Ag^+ ions is unwanted include those where AgNPs are used as imaging agents for X-ray CT,[70,71] photoacoustic,[72] and optical coherence tomography (OCT)[73] or incorporated into devices such as orthopedic implants,[74] or used as drug delivery vehicles.[75,76] AgNP-based imaging agents that undergo surface oxidation and Ag^+ ion dissolution result in a change in the size and shape, which are physicochemical features that affect the optical and light scattering properties of AgNPs.[77,78] Besides, when AgNP-based drug delivery agents undergo surface oxidation and Ag^+ ion dissolution, AgNPs become unstable, have short shelf-life, undergo premature drug release, and induce toxicity. Therefore, in these types of applications, robust AgNPs that do not undergo surface oxidation and Ag^+ ion release are of paramount importance to minimize any human health and safety concerns.

To protect the AgNPs from surface oxidation and instability, AgNPs have been modified with covalent organic ligands such as polyvinylpyrrolidone (PVP),[64] lipids,[70] and polyethylene glycol (PEG),[79–82] or thiolated PEG[83] as well as inorganic substrates such as gold[79] or silica core–shell.[84,85] Alloys comprised of silver, gold, and chromium have also been shown to enhance the stability of AgNPs[79,86] or other metal oxides.[87] Depending on the type of AgNPs and method of surface protection, stability studies show that the AgNPs are stable from 1 week to 100 days without a change in the size or shape in water or citrate buffer.[70,79,86] AgNPs with the organic surface coating are not very stable for long periods compared to those with an inorganic surface layer that shields the AgNP core. These design strategies are great steps towards controlling Ag^+ ion dissolution and preventing AgNPs from undergoing surface oxidation in a variety of media. However, these methods require more than one step, are complicated, and are limited to one shape or size of AgNPs. In addition, the organic ligands are not as protective and might limit their use in different applications. Opportunities remain for simple and inexpensive methods with few steps to produce versatile, stable, and biocompatible AgNPs of varying size and shape that do not undergo surface oxidation, Ag^+ ion release, and shape conversion.

In this study, a simple, innovative, and versatile approach to the design of water-soluble AgNPs that are differentially shielded from surface oxidation and Ag^+ ion dissolution is described. These AgNPs have a bioorganic surface coating comprised of natural lipid membranes that are anchored to the AgNP surface by a stoichiometric number of hydrophobic thiols (Scheme 1). These hybrid lipid-coated AgNPs and their stability were characterized and evaluated using UV-Visible (UV-Vis) spectroscopy, inductively coupled plasma mass spectrometry (ICP-MS), and transmission electron microscopy (TEM) to demonstrate that the hybrid lipid membrane shields the AgNP to prevent surface oxidation, Ag^+ ion release, and shape or size conversion. The hybrid lipid-membrane coating is adaptable and can be used to coat AgNPs of varying size and shape for controlled release or no release of Ag^+ ions. A wide variety of commercially available

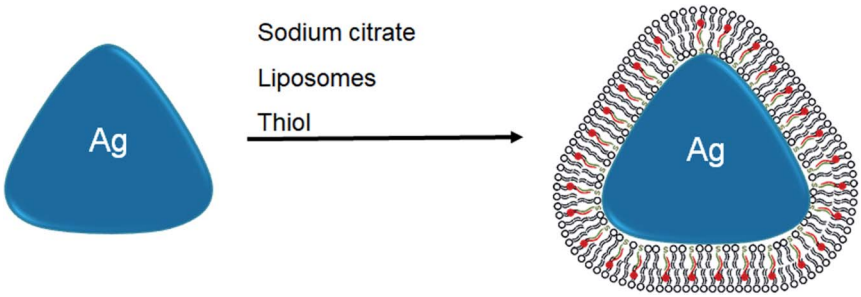

Scheme 1 Assembly of robust hybrid lipid-coated AgNPs.

lipids with different functional groups, conjugated dyes or drugs, and other ligands can be used to coat the AgNPs. This adaptable design allows one to produce a library of membrane-coated AgNP with tuned surface chemistry and optical properties for a variety of applications. For example, the hybrid lipid-coated AgNPs can be used in clinical applications where AgNPs are used as drug delivery and bioimaging agents and where degradation of AgNPs from surface oxidation, Ag^+ ions, shape conversion is unwanted. Furthermore, robust AgNPs that do not release Ag^+ ions are now available for toxicological studies where the effect of shape, size, and surface area on toxicity can be studied.

Results and discussion

Preparation of shaped-locked silver nanoparticles (AgNPs)

Previously we showed that hybrid lipid-coated gold nanoparticles (AuNPs) have unique stability in the presence of strong etchants such as cyanide (CN^-)[88–91] when compared to other AuNPs with less robust coatings, such as citrate and thiols, that typically undergo rapid oxidation in the presence of CN^-.[92–94] In addition to hybrid lipid-coated AuNPs, traditionally AuNPs are more stable to oxidation compared to silver nanoparticles (AgNPs) that are not as stable and undergo surface oxidation readily. Therefore, to test the versatility of hybrid lipid membranes as a strategy to stabilize AgNPs, citrate-capped AgNPs are coated with the hybrid lipid membranes to shield them from surface oxidation ($Ag^0 \rightarrow Ag^+$) and Ag^+ ion release. The synthesis begins with the use of citrate-capped AgNPs of various sizes and shapes that are prepared using a modified procedure previously reported in the absence of polyvinylpyrrolidone (PVP).[78,95–97] Briefly, varying amounts of $NaBH_4$ are added to a solution containing a mixture of $AgNO_3$, sodium citrate, and H_2O_2 to generate spheres, rods, and triangular-shaped AgNPs. UV-Vis show a characteristic narrow localized surface plasmon resonance (LSPR) band at 405 nm for spherical AgNPs (Fig. 1A(i)) with an average diameter of 9.9 nm $\pm$ 4.4 nm as measured by TEM (Fig. 1B and S1A†) from 607 spherical nanoparticles. The UV-Vis spectra taken of rod-shaped AgNPs show a small characteristic shoulder LSPR at 408 nm and more intense band at 558 nm (Fig. 1A(ii)) with an average width of 5.9 $\pm$ 1.0 nm and length 20 $\pm$ 5.6 nm as measured by TEM (Fig. 1C and S1C†) from 232 nanorods. Similarly, triangular-shaped AgNPs had characteristic a small shoulder LSPR band at 440 nm and an intense band 647 nm with an average length of 32 $\pm$ 7.1 nm (Fig. 1D and S1B†) that was determined by measuring the edge length of the triangular-shaped AgNPs from the apex of the triangle to the base on all three sides of 527 nanoparticles (Fig. 1D). TEM also shows that the solutions of rod and triangular-shaped nanoparticles are not homogeneous in size and morphology (Fig. 1C and D) and contain mixtures comprised of spheres, triangles, and rods as evidenced by the broadness of the LSPR band. Analysis of TEM images showed that the triangular-shaped nanoparticle solutions are comprised of 35% spheres, 1% rods, and 64% triangles. There were many overlapping AgNPs in the rod-shaped solutions from the TEM imaging making it difficult to assess the percent of each type of shape present.

Using these citrate-capped AgNPs, a layer-by-layer assembly approach is used to encapsulate and stabilize bilayer liposomes around the AgNP core of various shapes and sizes. The first step to the layer-by-layer assembly involves the addition of sodium oleate (SOA), which acts as a hydrophobic binding partner to the hydrophobic thiol added in the last stage of the assembly to prevent AgNP aggregation (Scheme 1). The addition of SOA is followed by the addition of preformed liposomes comprised of zwitterionic PC lipids that keep the AgNPs soluble in an aqueous environment. In addition, unlike other syntheses of lipid-coated nanoparticles where an excess of lipids is used during the coating process, these hybrid lipid-coated AgNPs are prepared with minimal lipids to cover the surface of each nanoparticle of a given shape and diameter. This strategy minimizes the formation of "nanoparticle-free" liposomes and reduces the number of purification steps of the materials after synthesis. The last stage of the assembly involves the addition of a hydrophobic thiol such as propanethiol (PT), hexanethiol (HT) or decanethiol (DT) to form the hybrid-lipid-coated AgNPs. The number of lipids, SOA, and thiols estimated around each AgNP is based on the size and shape (see ESI†).

UV-Vis show that the addition of various ligands (SOA, PC, thiol) to the citrate-capped AgNPs leads to a slight red-shift in the LSPR band of the AgNPs of varying shapes and sizes. For example, a ~29 nm red-shift is observed upon the formation of the triangular-shaped Ag-SOA-PC-DT nanoparticles after layer-by-layer assembly (Fig. 2) The change in the LSPR band is indicative of a change in the index of refraction of the AgNPs upon displacement of the citrate ligands with SOA, PC, and thiol ligands (Scheme 1). Since the Ag-SOA-PC-DT remains

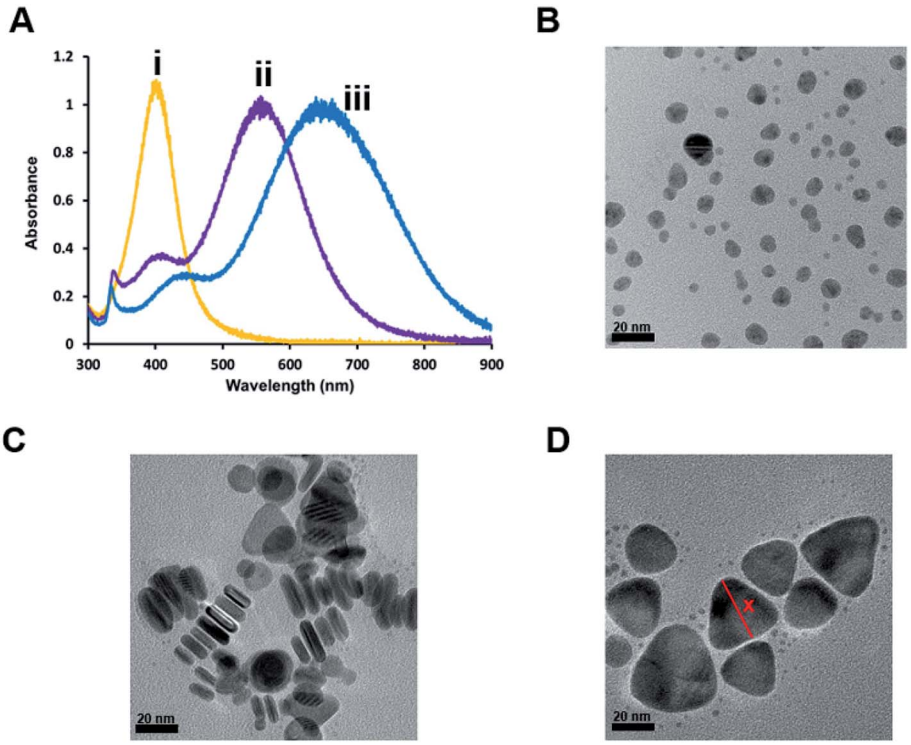

Fig. 1 (A) Representative UV-vis spectra of (i) spherical, (ii) rod-shaped, and (iii) triangular-shaped citrate-capped AgNPs in H_2O. Representative TEM micrographs of (B) spherical, (C) rod, and (D) triangular-shaped citrate-capped AgNPs with a reference to how measurements were taken (*x*). Scale bar = 20 nm.

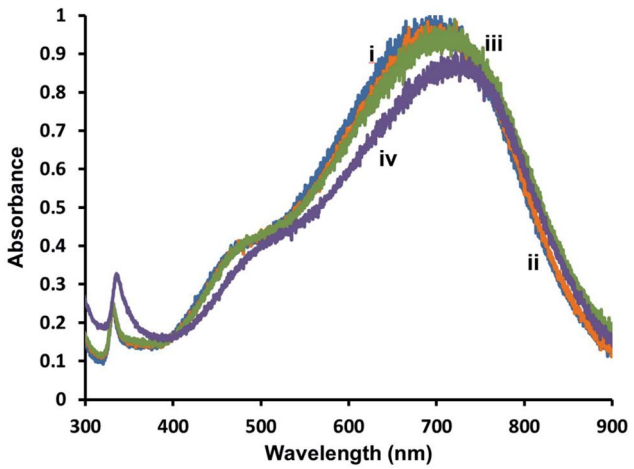

Fig. 2 Representative UV-Vis spectra showing the layer-by-layer assembly of 1 mL of triangular-shaped AgNPs (1.0 optical density (O.D.)) comprised of (i) Ag-citrate (blue), (ii) Ag-citrate-SOA (orange), (iii) Ag-citrate-SOA-PC (green), and (iv) Ag-citrate-PC-SOA-DT (purple) in H_2O.

soluble in an aqueous environment, this suggests that a bilayer is formed around the AgNP core whereby the zwitterionic polar headgroups of the second lipid layer is oriented away from the surface to interact with water molecules. Note that the addition of a stoichiometric amount of thiol does not result in any significant etching of the AgNP core as indicated by a lack of blue-shift in the LSPR band (Fig. 2(iii)).

Evidence of complete membrane coverage of AgNPs

To determine if the AgNPs are completely covered by lipid membranes and to examine their stability in the presence of oxidants, hybrid lipid-coated AgNPs were exposed to CN^-, which is known to oxidize metals such as Au^0 and Ag^0 to Au^{3+} or Ag^+, respectively.[98,99] Briefly, CN^- is added to a 1 mL solution of triangular-shaped AgNPs (1.2 Optical Density (O.D.)) and the UV-Vis spectra recorded before and after CN^- addition (Fig. 3). When CN^- is added to Ag-SOA-PC with no thiol ligands an immediate decrease in the LSPR band is observed (Fig. 3(i)), while no significant decrease in the SPR is observed over 24 h with Ag-SOA-PC-HT containing SOA, PC, and thiols, (Fig. 3(ii) and (iii)) or Ag-SOA-HT containing, SOA and thiols, (Fig. S2(ii)†). The lack of change in the LSPR band indicates that the AgNP surface is completely covered by lipids, thiols, and SOA molecules in a tightly packed arrangement such that CN^- ions are not able to penetrate the bilayer to etch the AgNP surface and is similar to that observed with hybrid lipid-coated AuNPs.[88–91] Although both the Ag-SOA-HT and Ag-SOA-PC-HT are found to be stable in the presence of CN^-, AgNPs with a combination of SOA, PC, and thiols are more soluble and stable (*vide infra*) long-term compared to AgNPs with SOA and thiols only. Similar protection of the AgNP surface is offered to spherical and rod-shaped hybrid lipid-coated AgNPs that do not undergo surface oxidation or shape conversion (Fig. S3†). To the best of our knowledge, this is the first time AgNPs of varying shapes and sizes have been shape-locked and shielded from surface

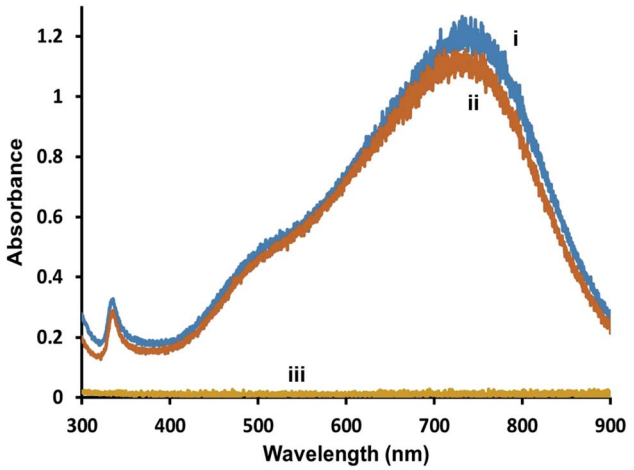

Fig. 3 Representative UV-vis spectra of triangular-shaped Ag-SOA-PC-HT (O.D. = 1.2) (i) before and (ii) after the addition of KCN, and (iii) Ag-SOA-PC after KCN in 10 mM sodium phosphate buffer pH 8.

oxidation and Ag^+ ion release using a hybrid lipid membrane coating. This design strategy, using thiol ligands as anchors is versatile and can be used to stabilize AgNPs from surface oxidation to produce robust AgNP platforms that can be employed for use in a variety of biomedical applications and for use in toxicological studies without the presence of Ag^+ ions as a confounding factor thereby minimizing their toxicity.

Impact of thiol chain length and surfactants on the stability of lipid-coated AgNPs

Previous studies showed that the length of the hydrocarbon backbone of the thiol and structure impacts the stability of hybrid lipid-coated AuNPs.[89] Similarly, to investigate if the thiol chain length impacts the stability and robustness of hybrid lipid-coated AgNPs, samples of Ag-SOA and Ag-SOA-PC are incubated with thiols (PT, HT, and DT). CN^- is then added to each of these hybrid lipid-coated AgNPs and the change in the LSPR and O.D. monitored (Fig. 4). Representative UV-Vis spectra of Ag-SOA-thiol and Ag-SOA-PC-thiol samples before and after CN^- addition show a significant red-shift in the LSPR band and decrease in O.D. with Ag-SOA-PT (~33% Δ in LSPR and ~95% Δ in O.D.) and Ag-SOA-PC-PT (~15% Δ in LSPR and 48% Δ in O.D.). In contrast, minimal change in the LSPR and O.D. of Ag-SOA-HT (~6% Δ in LSPR and 12% Δ in O.D.), Ag-SOA-PC-HT (~3% Δ in LSPR and ~7% Δ in O.D.), Ag-SOA-DT (~2% Δ in LSPR and ~2% Δ in O.D.), Ag-SOA-PC-DT (~2% Δ in LSPR and ~3% Δ in O.D.) is observed (Fig. 4). Overall, the Ag-SOA-thiol nanoparticles are found to be less stable than the Ag-SOA-PC-thiol nanoparticles demonstrating that the hybrid bilayer protects the surface from strong oxidants and keeps them stable in aqueous media.

This study confirms that long-chain hydrophobic thiols provide greater stability to the nanoparticles by helping to anchor the membranes close to the AgNP surface in a tight packing arrangement (Scheme 2A). In contrast, the short-chained PT is unable to fully interdigitate into the lipid bilayer to interact with the hydrophobic lipid tails to anchor the membrane close to the AgNP core (Scheme 2B). Hence, Ag-SOA-PC-PT nanoparticles are susceptible to surface oxidation and CN^- etching (Fig. 4). A ranking of the AgNP stability in the presence of CN^- with thiols of varying chain lengths from greatest to least stable are DT ≥ HT > PT and is consistent with previous work.[89] These studies show that differentially shielded nanoparticles can be prepared by varying the thiol chain lengths to control the release of Ag^+ ions.

To further test the robustness of the hybrid lipid-coated AgNPs against susceptibility to surface oxidation, nanoparticle samples were exposed to a well-known membrane disrupting surfactant, TWEEN®20. To ensure that liposome disruption occurred, four times the critical micelle concentration (CMC) of TWEEN®20 (PC : TWEEN®20 ratio is 1 : 15) was incubated for 30 min with a 1 mL sample of triangular-shaped Ag-SOA-PC-PT or Ag-SOA-PC-HT nanoparticles of 1.0 O.D. in H_2O. Samples are exposed to CN^- and monitored by UV-Vis spectroscopy over 1 week (Fig. 5). Minimal change in the O.D. (<1%) is observed upon the addition of TWEEN®20 to Ag-SOA-PC-HT with the long-chained hydrophobic thiol (Fig. 5A(ii)), while a significant change (>98%) is observed Ag-SOA-PC-PT with the short-chained thiol (Fig. 5B(ii)). An additional 40–51% decrease in O.D. is observed with Ag-SOA-PC-PT in the presence of TWEEN®20 and CN^- when compared to Ag-SOA-PC-PT and Ag-SOA-PT in the presence of CN^- and absence of TWEEN®20. This indicates that TWEEN®20 can disrupt the structural integrity of the membrane surrounding Ag-SOA-PC-PT to enable greater

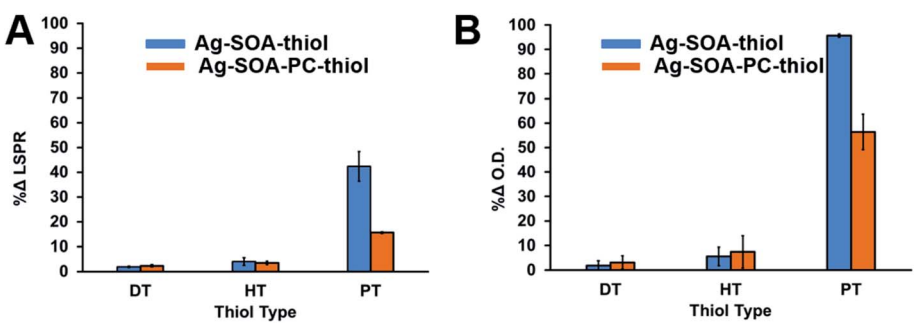

Fig. 4 Representative |% change| in the (A) LSPR band and (B) O.D. of Ag-SOA-thiol (blue) or Ag-SOA-PC-thiol (orange) nanoparticles 24 h after the addition of 20 μL of 307 mM KCN in 10 mM sodium phosphate buffer pH 8. DT = decanethiol, HT = hexanethiol, and PT = propanethiol.

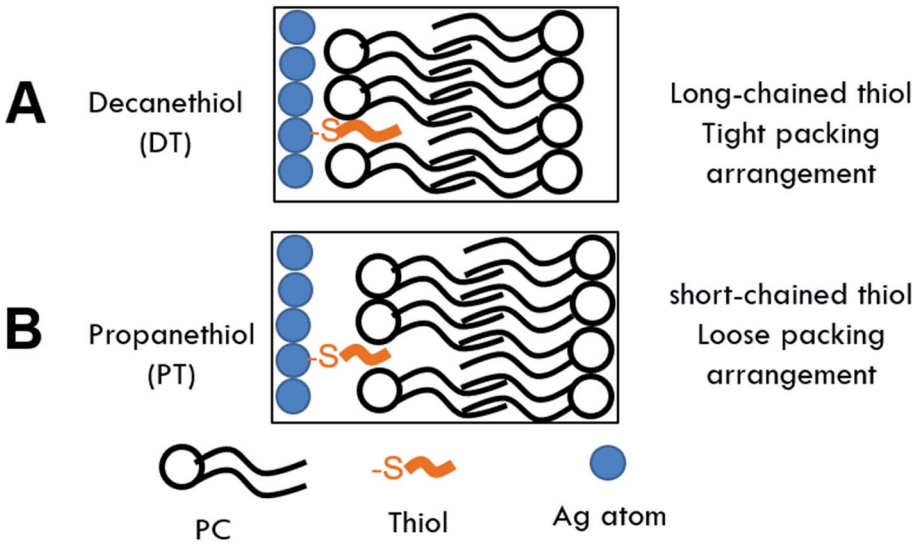

Scheme 2 Cartoon of hybrid lipid-membrane composition around AgNP core containing (A) decanethiol (DT) and (B) propanethiol (PT).

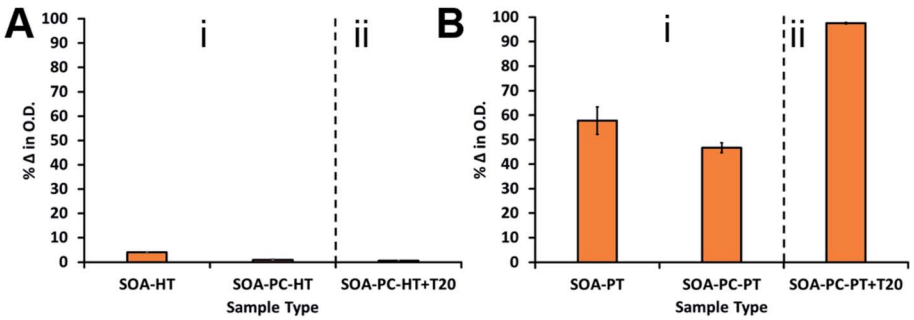

Fig. 5 A comparison of the percent change in the O.D. of (A) Ag-SOA-HT and Ag-SOA-PC-HT (i), and Ag-SOA-PC-HT with TWEEN®20 (ii), and (B) Ag-SOA-PT, Ag-SOA-PC-PT (i), and Ag-SOA-PC-PT with TWEEN®20 (ii). All samples are monitored for 1 week post-KCN addition. The final concentration of TWEEN®20 in all samples is 0.2 mM.

penetration of CN^- for etching. Most importantly, this study suggests that membrane disrupting surfactants are unable to disrupt the structural integrity of hybrid lipid membranes that are tightly packed with long-chained hydrophobic thiols (Ag-SOA-PC-HT) (Scheme 2A) and completely shields the AgNP surface from oxidation and Ag^+ ion dissolution.

Long-term storage stability and Ag^+ ion dissolution

The control of Ag^+ dissolution is an important feature of AgNPs that defines their use as antimicrobials, drug delivery, imaging agents, and toxicity studies. Therefore, it is important to evaluate the long-term storage of AgNPs and their ability to undergo Ag^+ ion release *via* surface oxidation over time. UV-Vis spectroscopy and ICP-MS was used to study the long-term stability of the most stable triangular-shaped Ag-SOA-thiol and Ag-SOA-PC-X (thiol = PT, HT, DT) platforms. Briefly, the UV-Vis spectra were recorded for AgNP platforms prepared and stored in H_2O in the dark at 25 °C over 2 months under aerobic conditions (Fig. 6). The % change in the O.D. (Fig. 6A and B) and LSPR (Fig. S4†) of Ag-SOA-PC-X (X = PT, HT, DT) is minimal after 21 days of storage indicating that hybrid lipid-coated AgNPs are stable and soluble with no surface oxidation, Ag^+ ion dissolution, or shape conversion. TEM studies of a 2 month-old sample of triangular-shaped Ag-SOA-PC-HT showed an average edge length of 38 ± 9.4 nm of 547 nanoparticles that was similar to a fresh batch of AgNPs confirming that the shape did not change (Fig. 6C and D). While the Ag-SOA-DT and Ag-SOA-HT nanoparticles with no PC remained stable after 21 days, a 23% change in O.D. is observed for the Ag-SOA-PT platforms after 24 h followed by an additional 30% change in O.D. after 21 days. Similar changes are observed in the LSPR band of the Ag-SOA-PT confirming that these AgNPs are not as stable as the hybrid lipid-coated AgNPs (Fig. S4†). Ag-SOA-PT shows visible signs of aggregation as evidenced by a noticeable dark precipitate in the vial and loss of color, indicating that the Ag-SOA-PT underwent aggregation and surface oxidation. This is not surprising as short-chained alkanethiols are known to etch metal nanoparticles making the AgNPs less stable.[100]

ICP-MS studies were performed to confirm that Ag-SOA-PC-HT did not undergo surface oxidation and Ag^+ ion dissolution. Samples of spherical and triangular-shaped Ag-Cit, Ag-

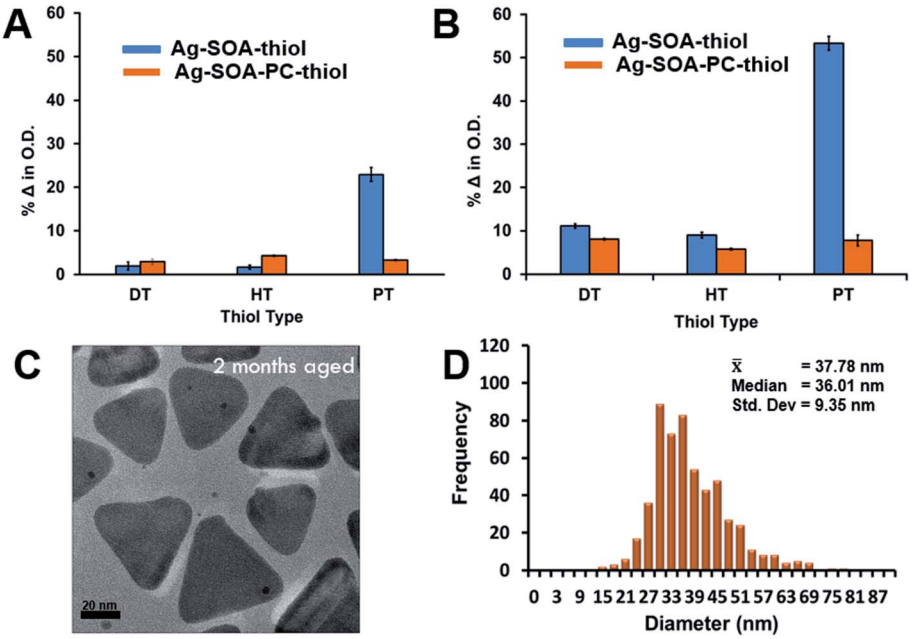

Fig. 6 Percent change in the O.D. of the triangular-shaped Ag-SOA-thiol (blue) and Ag-SOA-PC-thiol (orange) nanoparticles after (A) 1 day and (B) 21 days of preparation and storage in H_2O at 25 °C in the dark under aerobic conditions. (C) Representative (C) TEM image and (D) distribution histogram of triangular-shaped Ag-SOA-PC-HT nanoparticles after 2 months.

SOA-PC, Ag-SOA-PC-PT, and Ag-SOA-PC-HT were prepared in H_2O, purified by ultracentrifugation to remove any unreacted trace Ag^+ ions from the initial synthesis, and stored in the dark at 25 °C for 1 week. At each time point, 1 mL of spherical AgNP (1.2 O.D.) or triangular AgNPs (0.8 O.D.) samples were retrieved, filtered by ultracentrifugation using Vivaspin columns with PES membrane with a molecular weight cut-off (MWCO) of 3 kDa at 4700 rpm for 4 min, and the filtrate collected for ICP-MS analysis. Filtrates retrieved at all time points show the presence of Ag^+ ions for spherical and triangular-shaped Ag-Cit and Ag-Cit-SOA-PC nanoparticles within 1 h, 24, and 1 week (Fig. 7 and Tables S1, S2†). The Ag-SOA-PC shows the greatest amount of Ag^+ ion release because the SOA and the PC are not covalently attached making these nanoparticles more prone to surface oxidation compared to the citrated-capped AgNPs where the citrate oxygen groups are covalently attached. Additionally, spherical AgNPs released more Ag^+ ions compared to triangular-shaped AgNPs and is reasonable since spherical AgNPs have a larger surface to volume ratio and larger concentration of AgNPs compared to the triangular-shaped AgNPs. Not surprisingly, the hybrid lipid-coated AgNPs, Ag-SOA-PC-HT and Ag-SOA-PC-PT, showed minimal or no Ag^+ release over 1 week (Fig. 7 and Tables S1, S2†). The ICP-MS studies are consistent with the UV-Vis studies showing minimal % change of the O.D. (Fig. 6) and LSRP band (Fig. S5†) and are found to be similar for both spherical and triangular-shaped AgNPs. This study demonstrates that the surface coating surrounding the AgNP core significantly affects the release rate of Ag^+ ions. The more

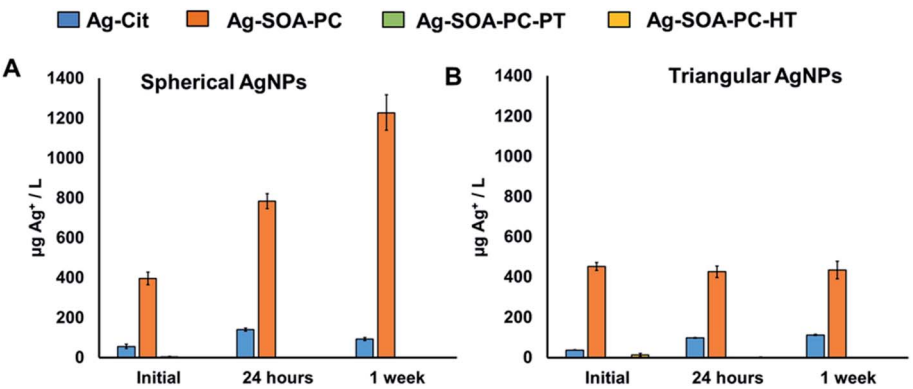

Fig. 7 ICP-MS analysis of Ag^+ ion release from 1 mL samples of (A) spherical AgNPs (1.2 O.D.) and (B) triangular shaped-AgNPs (0.8 O.D.) with Ag-Cit (blue), Ag-SOA-PC (orange), Ag-SOA-PC-PT (green), and Ag-SOA-PC-HT (yellow) compositions in stored in the dark aerobically in H_2O at 25 °C after initial synthesis, 24 h, and 1 week.

shielded the AgNPs, the more stable, and less prone to surface oxidation. Overall, AgNP platforms can be ranked from least shielded (less stable) to more shielded (more stable) in the following order of decreasing Ag^+ ion release: Ag-Cit < Ag-SOA-PC < Ag-SOA-PC-PT < Ag-SOA-PC-HT ≤ Ag-SOA-PC-DT.

Effect of chloride ions, pH, and thiolates on nanoparticle stability

AgNPs are incorporated into many different commercially available products that end up in environments where they can pose environmental and human health risks. Besides, since AgNPs can also be employed in biomedical applications their stability under physiologically relevant conditions is important. It is well-known that AgNP aggregation and destabilization is highly dependent on the surface coating and the environment that they are exposed to.[101–103] Most AgNPs suspensions are destabilized and are unstable in media containing thiols, disulfides, and high $CaCl_2$ or NaCl concentrations in the millimolar range as well as polysaccharides and proteins as they occur in freshwaters or biological media.[101,104–110] In cellular environments AgNPs are taken up in lysosomes after phagocytosis, where the potential to release of Ag^+ ions is greater at lower pH.[111–113] Furthermore, in toxicological studies aggregation significantly affect the dose–response, nature of the toxicant (AgNPs *vs.* aggregated AgNPs), and exposure route. While protective surface coatings can stabilize AgNPs, it is important to test and monitor AgNP aggregation and the rate of Ag^+ dissolution, which is dependent on pH,[103,114] presence of thiols,[115,116] surface coating, size of the AgNPs,[117] and increase in O_2 content.[103,118] Therefore, to test the stability and robustness of Ag-SOA-PC-HT, samples were monitored over time after exposure to sources of chlorides, disulfides, thiolates, and varying pH conditions. For these studies, purified Ag-SOA-PC-HT was used to ensure free ligands (citrate, lipids, thiols, *etc.*) that could play a role in aggregation or surface oxidation is completely removed. Prior to purification, CN^- etch test confirmed that the triangular-shaped Ag-SOA-PC-HT are stable and completely shielded from surface oxidation.

To investigate the stability of Ag-SOA-PC-HT at low pH conditions, 1 mL aliquots of triangular-shaped Ag-SOA-PC-HT at 0.8 O.D. were exposed to 2 M HCl until the pH decreased to 7 or 5 and changes in the LSPR and the O.D. monitored at after 1 and 24 h. The stability of the AgNPs is studied at pH 5 to simulate lysosomal fluid and tumor microenvironments where AgNPs reside. At pH 7 very minimal change in O.D. and LSPR is observed, indicating that the hybrid lipid-coated AgNPs are stable at physiologically relevant pH (Fig. 8A). However, at pH 5, a noticeable decrease in the O.D., 36% after 1 h and 53% after 24 h are observed (Fig. 8A), which indicates that the Ag-SOA-PC-HT is aggregating. There is also a slight blue-shift (7%) in the LSPR band at pH 5, suggesting that the Ag-SOA-PC-HT is also undergoing a minimal amount of Ag^+ ion dissolution within the first hour and does not change to any significant degree after 24 h (Fig. S6†). This specifies that the Ag-SOA-PC-HT is relatively stable at low pH and does not undergo any rapid and significant surface oxidation and Ag^+ ion release. Evidence of aggregation is further confirmed by visible dark precipitates that are observed when the zwitterionic polar head groups are protonated making the Ag-SOA-PC-HT nanoparticles less soluble. The instability due to aggregation is more evident by the significant decrease in the O.D. when the pH drops to pH 2 (Fig. S6†). In contrast, AgNPs with Cit and SOA-PC are not stable in the presence of 2 M HCl, which aggregate and undergo Ag^+ ion dissolution rapidly. The hybrid lipid coating anchored with PT or DT shields the AgNPs from undergoing rapid Ag^+ ion dissolution that is observed with elemental Ag-based nanoparticles and Ag_2S nanoparticles coated with a lipid and lipid-PEG layer that leach more Ag^+ at lower pH.[70,103,119] Consequently, the relative stability at physiological and pH 5 introduces Ag-SOA-PC-HT nanoparticles as a potential platform for bioimaging or drug delivery applications lessening concerns that the AgNPs will undergo Ag^+ ion dissolution in lysosomal compartments once taken up into cells and induce toxicity.

To investigate the stability of Ag-SOA-PC-HT under high ionic strength conditions, 1 mL aliquots of triangular-shaped Ag-SOA-PC-HT at 0.8 O.D. were exposed to varying NaCl and $CaCl_2$ concentrations and the change in the LSPR and O.D. monitored after 1 and 24 h. Upon exposure to increasing concentrations of NaCl (50–150 mM), Ag-SOA-PC-HT shows a 2–14% decrease in the O.D. within 1 h and an 11–52% decrease in O.D. within 24 h (Fig. 8B). A minimal shift (<1%) in the LSPR band over increasing concentrations is observed indicating no

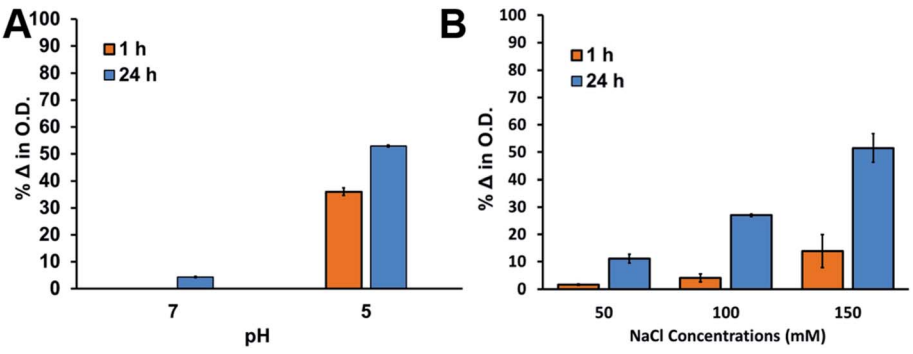

Fig. 8 Percent change in the O.D. of the triangular-shaped Ag-SOA-PC-HT after 1 h (orange) and 24 h (blue) upon varying (A) the pH (5 and 7) and (B) concentrations of NaCl from 50 mM to 150 mM in H_2O at 25 °C.

change in the size or shape of the AgNPs within 1 h (Fig. S7†). Similarly, when 50 mM of $CaCl_2$ is added to purified Ag-SOA-PC-HT, a 16% decrease in the O.D. and very small red-shift in the LSPR band (0.7%) is observed within 1 h (Fig. S8†) indicating AgNP aggregation. The observed aggregation in the presence of 50 mM of $CaCl_2$ is consistent with other studies where Ca^{2+} is known to interact with the phosphate groups of lipids and carbonyl groups of the polar head group.[120–124] Consequently, it is expected that under high concentrations of Ca^{2+} bridging interactions between Ca^{2+} and lipid-coated AgNPs occur, leading to AgNP aggregation that is somewhat reversible in the presence of EDTA (Fig. S8†). The lack of change in the LSPR band, with increasing concentrations of NaCl (>50 mM), indicates that Ag-SOA-PC-HT is aggregating under high salt concentrations. That is, a lack of a blue-shift in the LSPR band suggests that there is no surface oxidation and shape conversion of the triangular Ag-SOA-PC-HT as a result of Ag^+ ion release caused by Cl^- etching at high energy points.[110,125] The robust nature of the shielded Ag-SOA-PC-HT nanoparticles is a physicochemical feature that is important for future use *in vivo*, toxicological assessment, and for minimizing the effect of Ag^+ ions released form AgNPs in the environment.

In contrast, these observations differ significantly from that of spherical and triangular citrate-capped AgNPs that readily etch in the presence of 50 mM NaCl, resulting in rapid and dramatic changes to both the LSPR and O.D. (Fig. 9(A and D)) and a change in color from yellow (spherical) or blue (triangular) to colorless (Fig. S9†). The rapid change in the LSPR and O.D. is indicative of Cl^- ion oxidation of Ag^0 to Ag^+ ions.[55,59] Citrate capping agents offer no protection to Cl^- oxidation of the AgNPs. The triangular and spherical Ag-Cit-SOA-PC without thiols underwent slower surface oxidation and Ag^+ ion dissolution. For the spherical Ag-Cit-SOA-PC a dramatic 26% decrease in the O.D. and loss of intensity of a golden yellow to a pale yellow color is observed after 1 week indicating surface oxidation (Fig. 9(B, E) and S9(E)†). The triangular Ag-Cit-SOA-PC

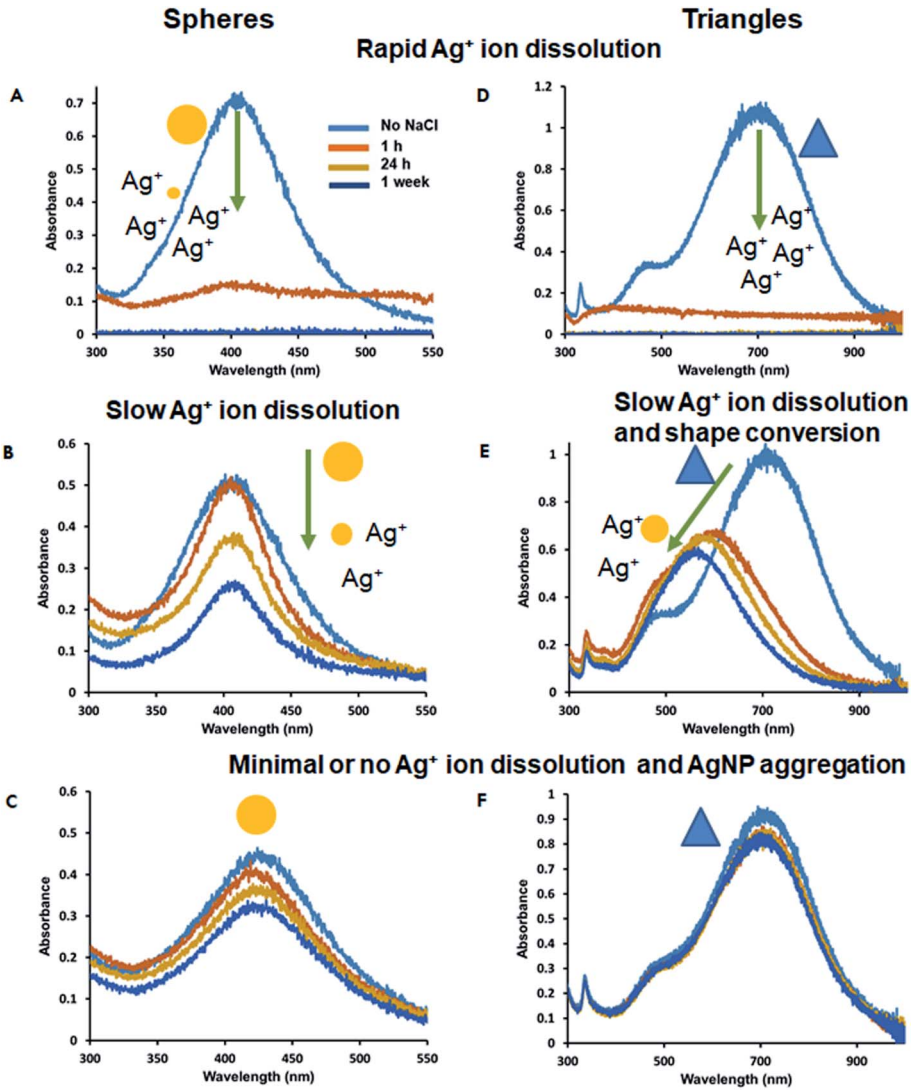

Fig. 9 UV-vis spectra of spherical (A) Ag-Cit, (B) Ag-Cit-SOA-PC, (C) Ag-Cit-SOA-PC-HT and triangular (D) Ag-Cit, (E) Ag-Cit-SOA-PC, (F) Ag-Cit-SOA-PC-HT in the absence and presence of 50 mM of NaCl in H_2O at 25 °C after 1 h, 24 h, and 1 week.

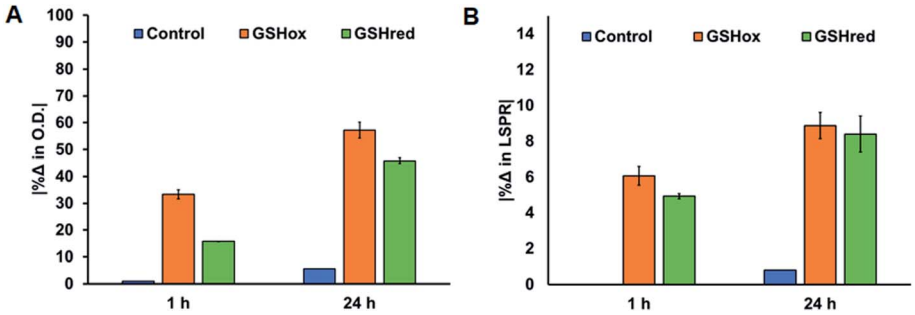

Fig. 10 Percent change in the (A) O.D. and (B) LSPR band of the triangular-shaped Ag-SOA-PC-HT nanoparticles before (blue) and after the addition of 50 mM GSH_{ox} (orange) and GSH_{red} (green) after 1 h and 24 h in H_2O at 25 °C.

nanoparticles showed a 150 nm blue-shift in the LSPR band and a 41% decrease in the O.D. after 1 week and a change in color from dark blue to purple after 1 hour and lighter shades of purple after 24 hours to 1 week (Fig. 9(B, E) and S9(F)†). This change in O.D., LSPR, and color is indicative of surface oxidation and shape conversion from triangles to large spherical-shaped AgNPs or complete decomposition. The AgNPs with SOA and PC offered more protection with slower Ag^+ ion release over time compared to citrate ligands (Fig. 9(B and E)). Not surprisingly, the spherical and the triangular-shaped hybrid lipid-coated Ag-Cit-SOA-PC-HT had minimal or no change in LSPR, O.D., or color confirming that the hybrid lipid membrane shields the surface from oxidation by Cl^- ions and Ag^+ ion release and is consistent with that observed in the presence of CN^- (Fig. 9(D and F)).

Lastly, to evaluate the stability of the Ag-SOA-PC-HT nanoparticles in the presence of thiolates and disulfides, which are found in biological environments in high concentrations and can increase the dissolved concentrations of free Ag^+ ions, samples were exposed to biological thiolates.[115] Briefly, 1 mL samples of Ag-SOA-PC-HT of 0.8 O.D. were exposed to reduced glutathione (GSH_{red}) or oxidized glutathione (GSH_{ox}) and the UV-Vis spectrum recorded (Fig. 10). After 1 h of exposure to GSH_{ox}, a 33% decrease in O.D. is observed while a 16% decrease in O.D. is observed in the presence of GSH_{red}. After 24 h, there was an additional 30% decrease in O.D. for GSH_{ox} and GSH_{red}. While an overall decrease in the O.D. was observed for Ag-SOA-PC-HT, there was a minimal shift in the LSPR band, indicating that there is some slight aggregation of Ag-SOA-PC-HT nanoparticles. More importantly, there was no evidence that a chemical reaction between the AgNPs and the GSH_{ox} occurred to oxidize the surface of the Ag-SOA-PC-HT to release Ag^+ ion and form GSH_{red}. These results suggest that the tight membrane packing around the AgNP core shields the surface from direct contact of GSH_{ox} with the AgNP surface oxidation further demonstrating that the Ag-SOA-PC-HT is a robust platform for biological applications.

Conclusions

Here robust hybrid lipid-coated AgNPs comprised of a lipid membrane anchored by long-chained hydrophobic thiols were synthesized using a layer-by-layer assembly approach. The approach uses natural lipids as biocompatible capping ligands to shield the AgNP core from surface oxidation, Ag^+ ion release, aggregation, and shape conversion. Furthermore, for the first time, this strategy allows for the design of stable and soluble AgNPs that are "shaped-locked" so there is no shape conversion or degradation of the AgNPs where the AgNPs would lose their unique optical, electronic, or catalytic properties that are based on shape or size.

The robustness of the Ag-SOA-PC-HT nanoparticles, as interrogated by CN^- etch studies, demonstrates that the membrane encapsulating the AgNP completely covers the AgNP core protecting it from surface oxidation even in the presence of membrane disrupting surfactants such as Tween®20. UV-Vis and ICP-MS studies confirm that the protective coating shields the AgNPs from surface oxidation over months with no Ag^+ ion release even under harsh biological and environmental media conditions containing sources of chlorides, thiolates, disulfides, and low pH. The robustness of the AgNPs is dependent on the rigidity of the surface coating surrounding the AgNPs, and can be ranked in the order of stability from least shielded (less stable) to more shielded (more stable) in the following order: Ag-Cit < Ag-SOA-PC < Ag-SOA-PC-PT < Ag-SOA-PC-HT ≤ Ag-SOA-PC-DT. Their incredible stability is dependent on the chain-length of the thiol, where AgNPs with short-chained thiol anchors are less stable than those with long-chained hydrophobic thiols.

Because the rigidity of the membrane composition can be tuned to control Ag^+ ion release, opportunities exist for greater control of Ag^+ ion release over time, an important feature of antimicrobial agents embedded in textiles, food packaging, bandages, and stents. For the first time, robust lipid-coated AgNP platforms of varying sizes and shapes that do not undergo surface oxidation and Ag^+ ions are available for use in toxicological studies. These platforms now make it possible to evaluate and elucidate how the physicochemical features, size, shape, surface, coating, surface area, play a role in nanomaterial toxicity and nanoparticle–biological interactions. That is, how the physical properties of silver nanomaterials impact human health and ecotoxicity.

Lastly, these types of robust platforms are ideal for use as safe and biocompatible X-ray imaging and OCT contrast agents

whose optical and physical properties are not expected to change because of surface oxidation in biological environments. The lipid membrane composition of hybrid lipid-coated AgNPs can be easily modified by conjugation to incorporate cleavable molecular drugs, MRI contrast agents, or fluorescent molecules for bimodal imaging. Consequently, this facile surface modification makes this platform much more multifunctional and versatile for a range of biomedical applications without the concern of toxic Ag^+ ions being released from the surface that can impact human health compared to existing AgNP platforms. That is, the design strategy is flexible and can be adapted for any shape and size of AgNP with any membrane composition, allowing for small libraries of nanoparticles to be produced for varying biomedical and commercial applications.

Methods and materials

Reagents

95% L-α-phosphatidylcholine (PC), sodium borohydride ($NaBH_4$), trisodium citrate ($Na_3C_6H_3O_7$), 1-decanethiol 96% (DT), 1-hexanethiol 95% (HT), and 1-propanethiol 99% (PT), Tween®20, gluthathione reduced (GSH_{red}) and oxidied (GSH_{ox}) are from Sigma Aldrich. Sodium oleate (SOA) 97% is purchased from Tokyo Chemistry Industry Co, Ltd. Silver nitrate ($AgNO_3$) is from G. Frederick Smith Chemical Co. and potassium cyanide (KCN) is from Mallinckrodt, while 30% Hydrogen Peroxide is from BDH Chemicals. All chemicals were used as received. Nanopure water was from a Milli-Q ultra-pure system. Ultracentrifugation was performed with a Thermo Scientific, Sorvall ST 40R at 4700 rpm using Vivaspin ultracentrifuge concentrators with a PES membrane (Vivaspin 20, MWCO = 10k).

Preparation of silver nanoparticles

Using a modified procedure, $AgNO_3$ (43 mL of a 0.109 mM in H_2O) is combined with H_2O_2 (120 μL of 30% w/w) and $Na_3C_6H_3O_7$ (3.68 mL of a 34.2 mM in H_2O) in a 250 mL Erlenmeyer flask covered with aluminum foil to protect the solution from light exposure. The mixture is allowed to stir at 600 rpm with a medium-sized stir bar for approximately 1 min before a freshly prepared aqueous solution of $NaBH_4$ (360 μL of 100 mM in H_2O) is rapidly added to the center of the reaction vortex in the flask. $NaBH_4$ addition to the solution results in a rapid color change for approximately 2–3 min changing from pale yellow to orange, to purple, and finally, a blue color that is indicative of triangular silver nanoplates (AgNPLs). The resulting solution is allowed to stir for an additional 10 min before it is covered and stored in the refrigerator at 4 °C overnight. The same procedure was employed to form silver nanospheres (AgNSs) and nanorods (AgNRs), with the volume of $NaBH_4$ reduced to 110 μL and 160 μL, respectively.

Preparation of PC-coated silver nanoparticles (Ag-OA-PC-HT)

To citrate-capped AgNPs (1 mL of nanoparticles of O.D. 1.2 at λ_{max} 705 nm in H_2O) was added a solution of SOA (1.1 μL of a 9.4 mM in H_2O) in an Eppendorf. The Ag-citrate-SOA solution was vortexed for 5 s and allowed to incubate for 20 min. This is followed by the addition of PC liposomes (10.4 μL of 0.32 mM in 10 mM sodium phosphate buffer pH 8) that was incubated with the Ag-SOA for 40 min after 5 s of vortex mixing. The PC liposome was prepared using a well-established method where a solution of PC (100 μL of 3.3 mM $CHCl_3$) was evaporated under a stream of N_2 as a thin film and placed under a vacuum of 12 h to remove trace organic solvents. The film was resuspended in 1 mL of 10 mM sodium phosphate buffer pH 8 and sonicated for 90 min until the solution was clear. To the Ag-citrate-SOA-PC solution was added a fresh solution of hexanethiol (1.4 μL of a 30 mM solution in ethanol) that were incubated for a minimum of 30 min before use. HT can be substituted for an equivalent amount of PT or DT to produced Ag-SOA-PC-PT or Ag-SOA-PC-HT nanoparticles. Because of their robust nature, the Ag-SOA-PC-HT or Ag-SOA-PC-DT nanoparticles can be purified to remove free citrate, PC, and SOA by incubating each 1 mL of hybrid-coated AgNPs with 10 μL of 10 mM of Tween®20 for 1 h before ultracentrifugation at 4700 rpm, using a Vivaspin 20 column (3 × 10 mL of H_2O).

Stability studies in the presence of cyanide, chloride salts, Tween®20, glutathione, and pH

To determine if the surface of the AgNPs are shielded from oxidation, we performed well-known cyanide (CN^-) etch test.[99] A 1 mL solution of triangular-shaped Ag-SOA-PC-HT (O.D. 1.2) is incubated with 20 μL of the 307 mM KCN in an Eppendorf for 1 h. The UV-Vis spectra were collected before and after the addition of KCN and the change in the O.D. and λ_{max} monitored.

Long-term storage stability was evaluated by storing stock solutions of spherical (O.D. 0.8) and triangular-shaped (O.D. 1.0) Ag-SOA-PC-HT in the dark at 25 °C. From these samples, 1 mL aliquots of AgNPs were retrieved and centrifuged using a Vivaspin column with PES membrane and MWCO of 3 kDa. Samples were centrifuged at 4700 rpm for 4 min and the filtrates collected for ICP-MS analysis at upon initial preparation, 24 h, and 1 week. The UV-Vis spectra were collected over time and the change in the O.D. and λ_{max} monitored.

To evaluate the stability of triangular-shaped Ag-SOA-PC-HT nanoparticles in the presence of membrane disrupting surfactants, chloride salts, pH, and biological thiols, 1 mL samples of AgNPs were incubated with Tween®20, NaCl, $CaCl_2$, GSH_{red} or GSH_{ox} and the pH varied between 2–8. To test the effect of membrane disrupting surfactants, 1 mL of triangular-shaped Ag-SOA-X or Ag-SOA-PC-X (O.D. = 1.0) (X = PT, HT, or DT) in 10 mM sodium phosphate buffer pH 8 were incubated with 20 μL of 10 mM Tween®20 for a final concentration 0.2 mM in the dark at 25 °C and allowed to incubate for 24 h before the addition of 20 μL of 307 mM KCN. The UV-Vis spectra were recorded before and after 1 week of KCN addition. To evaluate the effect of chlorides, 1 mL of triangular-shaped Ag-SOA-PC-HT (O.D. 0.8) was exposed to NaCl or $CaCl_2$ to yield final concentrations of 50 mM, 100 mM, or 150 mM. To understand if the interactions of the nanoparticles exposed to $CaCl_2$ are reversible, 100 μL of 500 mM EDTA was added to the Ag-SOA-PC-HT nanoparticles exposed to 50 mM $CaCl_2$. Alternatively, to

evaluate the effect of pH on nanoparticle stability, 1 μL of 2 M HCl was added to 1 mL of triangular-shaped Ag-SOA-PC-HT (0.8 O.D.) to adjust the pH to 5, respectively from an initial pH 7–8. To evaluate the effect of biological thiols, 160 mM of GSH_{red} and GSH_{ox} was added to 1 mL of triangular-shaped Ag-SOA-PC-HT (0.8 O.D.) to yield a final concentration of 50 mM. Due to solubility constraints, the stock solution of GSH_{ox} was prepared in 10 mM sodium phosphate buffer at pH 8 and the GSH_{red} stock was prepared in nanowater. The percent change in the O.D. or LSPR was monitored by taking a UV-Vis spectrum before and after the addition of NaCl, $CaCl_2$, $GSH_{red\ and}$ GSH_{ox}, Tween®20, and varying pH.

Transmission electron microscopy (TEM) and UV-Vis spectroscopy

Samples were prepared by drop-casting dilute solutions of AgNPs onto carbon-coated (300 Å) Formvar films on copper grids (Ted Pella). Samples sat for 5 min before the excess sample is wicked off by with a piece of filter paper and the process was repeated 3 times. Transmission electron micrographs were acquired on a Tecnai F-20 FEI microscope using a CCD detector at an acceleration voltage of 200 kV. AgNP size and shape analysis were performed using ImageJ software. Absorbance measurements were performed with an Ocean Optics USB2000 UV-visible spectrophotometer using a 1.0 cm path length quartz cell.

ICP-MS studies

ICP-MS measurements were performed in the OHSU Elemental Analysis Core with partial support from the NIH instrumentation grant S10RR025512. Samples of AgNPs (1 : 9 ratio of AgNPs and H_2O) were prepared. Samples were diluted into 15 ml metal-free polypropylene tubes (VWR 89049-170 series) in the Client's lab. All samples, controls, calibration standards, and rinses were prepared in 1% HNO_3 (trace metal grade, Fisher)/0.5% HCl (trace metal grade, Fisher). ICP-MS analysis was performed using an Agilent 7700x equipped with an ASX 500 autosampler. The system was operated at a radio frequency power of 1550 W, an argon plasma gas flow rate of 15 L min^{-1}, Ar carrier gas flow rate of 0.9 L min^{-1}. Silver was measured in NoGas mode. Data were quantified using a 10-point (0, 0.5, 1, 2, 5, 10, 20, 50, 100, 500 ppb (μg kg^{-1})) calibration curve using a single-element standard (Ag, (VHG-LAGN-100, Lot # 404-0117-1)) in 1% HNO_3/0.5% HCl. For each sample, data were acquired in triplicates and averaged. A coefficient of variance (CoV) was determined from frequent measurements of a sample containing ~10 ppb Ag. An internal standard (Sc, Ge, Bi) continuously introduced with the sample was used to correct for detector fluctuations and to monitor plasma stability. Accuracy of the calibration curve was assessed by measuring NIST reference material (water, SRM 1643f) and found to within 5% of the expected value for Ag in all measurements except for the zebrafish samples where Ag recovery was 82%.

Abbreviations

AgNP	Silver nanoparticle
Cit	Citrate
SOA	Sodium oleate
PC	Phosphatidylcholine
HT	Hexanethiol
PT	Propanethiol
DT	Decanethiol
Ag^+	Silver ions
PVP	Polyvinylpyrrolidone
PEG	Polyethylene glycol
LSPR	Localized surface plasmon resonance
O.D.	Optical density
AuNP	Gold nanoparticle
CN^-	Cyanide
MWCO	Molecular weight cutoff
TEM	Transmission electron microscopy
CMC	Critical micelle concentration
GHS_{ox}	Oxidized glutathione
GSH_{red}	Reduced glutathione

Author contributions

The manuscript was written through the contributions of all authors. All authors have approved the final version of the manuscript.

Funding

This work was supported by NSF Grant #1762278.

Conflicts of interest

There are no conflicts to declare.

References

1 E. O. Simbine, L. d. C. Rodrigues, J. Lapa-guimarães, E. S. Kamimura, C. H. Corassin and C. A. F. d. Oliveira, Application of silver nanoparticles in food packages: a review, *Food Sci. Tech.*, 2019, **39**, 793–802.

2 K. Kraśniewska, S. Galus and M. Gniewosz, Biopolymers-Based Materials Containing Silver Nanoparticles as Active Packaging for Food Applications–A Review, *Int. J. Mol. Sci.*, 2020, **21**(3), 698.

3 W. Wang, Z. Yu, F. K. Alsammarraie, F. Kong, M. Lin and A. Mustapha, Properties and antimicrobial activity of polyvinyl alcohol-modified bacterial nanocellulose packaging films incorporated with silver nanoparticles, *Food Hydrocolloids*, 2020, **100**, 105411.

4 A. Kumar, P. K. Vemula, P. M. Ajayan and G. John, Silver-nanoparticle-embedded antimicrobial paints based on vegetable oil, *Nat. Mater.*, 2008, **7**(3), 236–241.

5 A. Desireddy, B. E. Conn, J. Guo, B. Yoon, R. N. Barnett, B. M. Monahan, K. Kirschbaum, W. P. Griffith,

R. L. Whetten, U. Landman and T. P. Bigioni, Ultrastable silver nanoparticles, *Nature*, 2013, **501**(7467), 399–402.

6 X. Sun, J. Shi, X. Zou, C. Wang, Y. Yang and H. Zhang, Silver nanoparticles interact with the cell membrane and increase endothelial permeability by promoting VE-cadherin internalization, *J. Hazard. Mater.*, 2016, **317**, 570–578.

7 Z. Huang, G. Chen, G. Zeng, Z. Guo, K. He, L. Hu, J. Wu, L. Zhang, Y. Zhu and Z. Song, Toxicity mechanisms and synergies of silver nanoparticles in 2,4-dichlorophenol degradation by Phanerochaete chrysosporium, *J. Hazard. Mater.*, 2017, **321**, 37–46.

8 J. I. Kwak and Y. J. An, Trophic transfer of silver nanoparticles from earthworms disrupts the locomotion of springtails (Collembola), *J. Hazard. Mater.*, 2016, **315**, 110–116.

9 V. K. Sharma, R. A. Yngard and Y. Lin, Silver nanoparticles: green synthesis and their antimicrobial activities, *Adv. Colloid Interface Sci.*, 2009, **145**(1–2), 83–96.

10 A. M. Fayaz, K. Balaji, M. Girilal, R. Yadav, P. T. Kalaichelvan and R. Venketesan, Biogenic synthesis of silver nanoparticles and their synergistic effect with antibiotics: a study against gram-positive and gram-negative bacteria, *Nanomedicine*, 2010, **6**(1), 103–109.

11 S. Chernousova and M. Epple, Silver as antibacterial agent: ion, nanoparticle, and metal, *Angew. Chem., Int. Ed.*, 2013, **52**(6), 1636–1653.

12 P. Mukherjee, A. Ahmad, D. Mandal, S. Senapati, S. R. Sainkar, M. I. Khan, R. Parishcha, P. V. Ajaykumar, M. Alam, R. Kumar and M. Sastry, Fungus-Mediated Synthesis of Silver Nanoparticles and Their Immobilization in the Mycelial Matrix: A Novel Biological Approach to Nanoparticle Synthesis, *Nano Lett.*, 2001, **1**(10), 515–519.

13 W. R. Li, X. B. Xie, Q. S. Shi, H. Y. Zeng, Y. S. Ou-Yang and Y. B. Chen, Antibacterial activity and mechanism of silver nanoparticles on Escherichia coli, *Appl. Microbiol. Biotechnol.*, 2010, **85**(4), 1115–1122.

14 S. Gurunathan, J. H. Park, J. W. Han and J. H. Kim, Comparative assessment of the apoptotic potential of silver nanoparticles synthesized by Bacillus tequilensis and Calocybe indica in MDA-MB-231 human breast cancer cells: targeting p53 for anticancer therapy, *Int. J. Nanomed.*, 2015, **10**, 4203–4222.

15 H. H. Lara, L. Ixtepan-Turrent, M. Jose Yacaman and J. Lopez-Ribot, Inhibition of Candida auris Biofilm Formation on Medical and Environmental Surfaces by Silver Nanoparticles, *ACS Appl. Mater. Interfaces*, 2020, DOI: 10.1021/acsami.9b20708.

16 F. Zhang, X. Wu, Y. Chen and H. Lin, Application of silver nanoparticles to cotton fabric as an antibacterial textile finish, *Fibers Polym.*, 2009, **10**(4), 496–501.

17 A. Verma, R. Arif and S. Jadoun, Synthesis, Characterization, and Application of Modified Textile Nanomaterials, in *Frontiers of Textile Materials*, ed. M. Shabbir, S. Ahmed and J. N. Sheikh, 2020, pp. 167–187, DOI: 10.1002/9781119620396.ch8.

18 S. Jodoun, A. Verma, and R. Arif, Modification of Textiles *via* Nanomaterials and Their Applications, in *Frontiers of Textile Materials*, ed. M. Shabbir, S. Ahmed and J. N. Sheikh, 2020, pp. 135–152, DOI: 10.1002/9781119620396.ch6.

19 A. Sood, M. S. Granick and N. L. Tomaselli, Wound Dressings and Comparative Effectiveness Data, *Adv. Wound Care*, 2014, **3**(8), 511–529.

20 K. Varaprasad, T. Jayaramudu, V. Kanikireddy, C. Toro and E. R. Sadiku, Alginate-based composite materials for wound dressing application:A mini review, *Carbohydr. Polym.*, 2020, **236**, 116025.

21 L. J. Wilkinson, R. J. White and J. K. Chipman, Silver and nanoparticles of silver in wound dressings: a review of efficacy and safety, *J. Wound Care*, 2011, **20**(11), 543–549.

22 M. E. El-Naggar, R. A. Soliman, O. M. Morsy and M. S. Abdel-Aziz, Nanoemulsion of Capsicum fruit extract as an eco-friendly antimicrobial agent for production of medical bandages, *Biocatal. Agric. Biotechnol.*, 2020, **23**, 101516.

23 J. Boateng and O. Catanzano, Silver and Silver Nanoparticle-Based Antimicrobial Dressings, in *Therapeutic Dressings and Wound Healing Applications*, ed. J. Boateng, 2020, pp. 157–184, DOI: 10.1002/9781119433316.ch8.

24 K. Wu, Y. Yang, Y. Zhang, J. Deng and C. Lin, Antimicrobial activity and cytocompatibility of silver nanoparticles coated catheters via a biomimetic surface functionalization strategy, *Int. J. Nanomed.*, 2015, **10**, 7241–7252.

25 D. Roe, B. Karandikar, N. Bonn-Savage, B. Gibbins and J. B. Roullet, Antimicrobial surface functionalization of plastic catheters by silver nanoparticles, *J. Antimicrob. Chemother.*, 2008, **61**(4), 869–876.

26 A. de Mel, K. Chaloupka, Y. Malam, A. Darbyshire, B. Cousins and A. M. Seifalian, A silver nanocomposite biomaterial for blood-contacting implants, *J. Biomed. Mater. Res., Part A*, 2012, **100**(9), 2348–2357.

27 S. Sivolella, E. Stellini, G. Brunello, C. Gardin, L. Ferroni, E. Bressan and B. Zavan, Silver Nanoparticles in Alveolar Bone Surgery Devices, *J. Nanomater.*, 2012, **2012**, 12.

28 S. P. Mulvaney, M. D. Musick, C. D. Keating and M. J. Natan, Glass-Coated, Analyte-Tagged Nanoparticles: A New Tagging System Based on Detection with Surface-Enhanced Raman Scattering, *Langmuir*, 2003, **19**(11), 4784–4790.

29 W. E. Doering, M. E. Piotti, M. J. Natan and R. G. Freeman, SERS as a Foundation for Nanoscale, Optically Detected Biological Labels, *Adv. Mater.*, 2007, **19**(20), 3100–3108.

30 A. Aygün, F. Gülbağça, M. S. Nas, M. H. Alma, M. H. Çalımlı, B. Ustaoglu, Y. C. Altunoglu, M. C. Baloğlu, K. Cellat and F. Şen, Biological synthesis of silver nanoparticles using Rheum ribes and evaluation of their anticarcinogenic and antimicrobial potential: A novel approach in phytonanotechnology, *J. Pharm. Biomed. Anal.*, 2020, **179**, 113012.

31 C. Loo, A. Lowery, N. Halas, J. West and R. Drezek, Immunotargeted Nanoshells for Integrated Cancer Imaging and Therapy, *Nano Lett.*, 2005, **5**(4), 709–711.

32 H. Kang, S. Jeong, Y. Park, J. Yim, B.-H. Jun, S. Kyeong, J.-K. Yang, G. Kim, S. Hong, L. P. Lee, J.-H. Kim, H.-Y. Lee, D. H. Jeong and Y.-S. Lee, Near-Infrared SERS Nanoprobes with Plasmonic Au/Ag Hollow-Shell Assemblies for In Vivo Multiplex Detection, *Adv. Funct. Mater.*, 2013, **23**(30), 3719–3727.

33 K. M. M. Abou El-Nour, A. a. Eftaiha, A. Al-Warthan and R. A. A. Ammar, Synthesis and applications of silver nanoparticles, *Arabian J. Chem.*, 2010, **3**(3), 135–140.

34 H. A. Atwater and A. Polman, Plasmonics for improved photovoltaic devices, in *Materials for Sustainable Energy*, Co-Published with Macmillan Publishers Ltd, UK, 2010, pp. 1–11.

35 S. H. Lee and B. H. Jun, Silver Nanoparticles: Synthesis and Application for Nanomedicine, *Int. J. Mol. Sci.*, 2019, **20**(4), 865.

36 L. Wei, J. Lu, H. Xu, A. Patel, Z.-S. Chen and G. Chen, Silver nanoparticles: synthesis, properties, and therapeutic applications, *Drug Discovery Today*, 2015, **20**(5), 595–601.

37 A.-C. Burduéşel, O. Gherasim, M. A. Grumezescu, L. Mogoantă, A. Ficai and E. Andronescu, Biomedical Applications of Silver Nanoparticles: An Up-to-Date Overview, *Nanomaterials*, 2018, **8**(9), 681.

38 S. Iravani, H. Korbekandi, S. V. Mirmohammadi and B. Zolfaghari, Synthesis of silver nanoparticles: chemical, physical and biological methods, *Res. Pharm. Sci.*, 2014, **9**(6), 385–406.

39 Y.-H. Chen and C.-S. Yeh, Laser ablation method: use of surfactants to form the dispersed Ag nanoparticles, *Colloids Surf., A*, 2002, **197**(1), 133–139.

40 V. Amendola and M. Meneghetti, Laser ablation synthesis in solution and size manipulation of noble metal nanoparticles, *Phys. Chem. Chem. Phys.*, 2009, **11**(20), 3805–3821.

41 C. Kinnear, T. L. Moore, L. Rodriguez-Lorenzo, B. Rothen-Rutishauser and A. Petri-Fink, Form Follows Function: Nanoparticle Shape and Its Implications for Nanomedicine, *Chem. Rev.*, 2017, **117**(17), 11476–11521.

42 Z. S. Pillai and P. V. Kamat, What Factors Control the Size and Shape of Silver Nanoparticles in the Citrate Ion Reduction Method?, *J. Phys. Chem. B*, 2004, **108**(3), 945–951.

43 J. Turkevich and G. Kim, Palladium: Preparation and Catalytic Properties of Particles of Uniform Size, *Science*, 1970, **169**(3948), 873–879.

44 J. Turkevich, Colloidal gold. Part I, *Gold Bull.*, 1985, **18**(3), 86–91.

45 T. C. Dakal, A. Kumar, R. S. Majumdar and V. Yadav, Mechanistic Basis of Antimicrobial Actions of Silver Nanoparticles, *Front. Microbiol.*, 2016, **7**, 1831.

46 M. M. Oliveira, D. Ugarte, D. Zanchet and A. J. G. Zarbin, Influence of synthetic parameters on the size, structure, and stability of dodecanethiol-stabilized silver nanoparticles, *J. Colloid Interface Sci.*, 2005, **292**(2), 429–435.

47 D. D. Evanoff Jr and G. Chumanov, Synthesis and optical properties of silver nanoparticles and arrays, *ChemPhysChem*, 2005, **6**(7), 1221–1231.

48 P. J. Goulet and R. B. Lennox, New insights into Brust-Schiffrin metal nanoparticle synthesis, *J. Am. Chem. Soc.*, 2010, **132**(28), 9582–9584.

49 B. Wiley, T. Herricks, Y. Sun and Y. Xia, Polyol Synthesis of Silver Nanoparticles: Use of Chloride and Oxygen to Promote the Formation of Single-Crystal, Truncated Cubes and Tetrahedrons, *Nano Lett.*, 2004, **4**(9), 1733–1739.

50 Y. Sun and Y. Xia, Shape-Controlled Synthesis of Gold and Silver Nanoparticles, *Science*, 2002, **298**(5601), 2176–2179.

51 B. J. Wiley, Y. Xiong, Z. Y. Li, Y. Yin and Y. Xia, Right bipyramids of silver: a new shape derived from single twinned seeds, *Nano Lett.*, 2006, **6**(4), 765–768.

52 H. Nhung Tran, T. H. Lien Nghiem, T. T. Duong Vu, V. Ha Chu, Q. Huan Le, T. M. N. Hoang, L. Thanh Nguyen, D. Minh Pham, K. Thuan Tong, Q. Hoa Do, D. Vu, T. Nghia Nguyen, M. Tan Pham, C. Nguyen Duong, T. Thuy Tran, V. Son Vu, T. T. Nguyen, T. B. Ngoc Nguyen, A. Duc Tran, T. T. Trinh and T. T. An Nguyen, Optical nanoparticles: synthesis and biomedical application, *Adv. Nat. Sci.: Nanosci. Nanotechnol.*, 2015, **6**(2), 023002.

53 C. Xue, G. S. Métraux, J. E. Millstone and C. A. Mirkin, Mechanistic Study of Photomediated Triangular Silver Nanoprism Growth, *J. Am. Chem. Soc.*, 2008, **130**(26), 8337–8344.

54 M. Gajbhiye, J. Kesharwani, A. Ingle, A. Gade and M. Rai, Fungus-mediated synthesis of silver nanoparticles and their activity against pathogenic fungi in combination with fluconazole, *Nanomedicine*, 2009, **5**(4), 382–386.

55 P. Bhuyar, M. H. A. Rahim, S. Sundararaju, R. Ramaraj, G. P. Maniam and N. Govindan, Synthesis of silver nanoparticles using marine macroalgae Padina sp. and its antibacterial activity towards pathogenic bacteria, *Beni-Suef University Journal of Basic and Applied Sciences*, 2020, **9**(1), 3.

56 H. A. Nasr, O. M. Nassar, M. H. El-Sayed and A. A. Kobisi, Characterization and antimicrobial activity of lemon peel mediated green synthesis of silver nanoparticles, *Int. J. Biol. Chem.*, 2020, (2), 56–63.

57 R. Banasiuk, M. Krychowiak, D. Swigon, W. Tomaszewicz, A. Michalak, A. Chylewska, M. Ziabka, M. Lapinski, B. Koscielska, M. Narajczyk and A. Krolicka, Carnivorous plants used for green synthesis of silver nanoparticles with broad-spectrum antimicrobial activity, *Arabian J. Chem.*, 2020, **13**(1), 1415–1428.

58 A. Aygün, S. Özdemir, M. Gülcan, K. Cellat and F. Şen, Synthesis and characterization of Reishi mushroom-mediated green synthesis of silver nanoparticles for the biochemical applications, *J. Pharm. Biomed. Anal.*, 2020, **178**, 112970.

59 J. Kadam, P. Dhawal, S. Barve and S. Kakodkar, Green synthesis of silver nanoparticles using cauliflower waste and their multifaceted applications in photocatalytic degradation of methylene blue dye and Hg2+ biosensing, *SN Appl. Sci.*, 2020, **2**(4), 738.

60 A. Kazlagić, O. A. Abud, M. Ćibo, S. Hamidović, B. Borovac and E. Omanović-Mikličanin, Green synthesis of silver

nanoparticles using apple extract and its antimicrobial properties, *Health and Technology*, 2020, **10**(1), 147–150.

61 M. Gomathi, A. Prakasam, P. V. Rajkumar, S. Rajeshkumar, R. Chandrasekaran and P. M. Anbarasan, Green synthesis of silver nanoparticles using Gymnema sylvestre leaf extract and evaluation of its antibacterial activity, *S. Afr. J. Chem. Eng.*, 2020, **32**, 1–4.

62 M. L. Guimarães, F. A. G. da Silva, M. M. da Costa and H. P. de Oliveira, Green synthesis of silver nanoparticles using Ziziphus joazeiro leaf extract for production of antibacterial agents, *Appl. Nanosci.*, 2020, **10**(4), 1073–1081.

63 H. G. Bhangale, S. G. Bachhav, K. M. Sarode and D. R. Patil, in *Green Synthesis of Silver Nanoparticles Using Mushroom Species, Their Characterization and Catalytic Activity*, Springer International Publishing, Cham, 2020, pp. 329–335.

64 D. E. Gorka, J. S. Osterberg, C. A. Gwin, B. P. Colman, J. N. Meyer, E. S. Bernhardt, C. K. Gunsch, R. T. DiGulio and J. Liu, Reducing Environmental Toxicity of Silver Nanoparticles through Shape Control, *Environ. Sci. Technol.*, 2015, **49**(16), 10093–10098.

65 K. T. Kim, L. Truong, L. Wehmas and R. L. Tanguay, Silver nanoparticle toxicity in the embryonic zebrafish is governed by particle dispersion and ionic environment, *Nanotechnology*, 2013, **24**(11), 0957–4484.

66 M. V. D. Z. Park, A. M. Neigh, J. P. Vermeulen, L. J. J. de la Fonteyne, H. W. Verharen, J. J. Briedé, H. van Loveren and W. H. de Jong, The effect of particle size on the cytotoxicity, inflammation, developmental toxicity and genotoxicity of silver nanoparticles, *Biomaterials*, 2011, **32**(36), 9810–9817.

67 I. Chopra, The increasing use of silver-based products as antimicrobial agents: a useful development or a cause for concern?, *J. Antimicrob. Chemother.*, 2007, **59**(4), 587–590.

68 J. N. Smith, D. G. Thomas, H. Jolley, V. K. Kodali, M. H. Littke, P. Munusamy, D. R. Baer, M. J. Gaffrey, B. D. Thrall and J. G. Teeguarden, All that is silver is not toxic: silver ion and particle kinetics reveals the role of silver ion aging and dosimetry on the toxicity of silver nanoparticles, *Part. Fibre Toxicol.*, 2018, **15**(1), 47.

69 C. Greulich, D. Braun, A. Peetsch, J. Diendorf, B. Siebers, M. Epple and M. Köller, The toxic effect of silver ions and silver nanoparticles towards bacteria and human cells occurs in the same concentration range, *RSC Adv.*, 2012, **2**(17), 6981–6987.

70 J. C. Hsu, P. C. Naha, K. C. Lau, P. Chhour, R. Hastings, B. F. Moon, J. M. Stein, W. R. T. Witschey, E. S. McDonald, A. D. A. Maidment and D. P. Cormode, An all-in-one nanoparticle (AION) contrast agent for breast cancer screening with DEM-CT-MRI-NIRF imaging, *Nanoscale*, 2018, **10**(36), 17236–17248.

71 P. C. Naha, K. C. Lau, J. C. Hsu, M. Hajfathalian, S. Mian, P. Chhour, L. Uppuluri, E. S. McDonald, A. D. Maidment and D. P. Cormode, Gold silver alloy nanoparticles (GSAN): an imaging probe for breast cancer screening with dual-energy mammography or computed tomography, *Nanoscale*, 2016, **8**(28), 13740–13754.

72 K. Homan, J. Shah, S. Gomez, H. Gensler, A. Karpiouk, L. Brannon-Peppas and S. Emelianov, Silver nanosystems for photoacoustic imaging and image-guided therapy, *J. Biomed. Opt.*, 2010, **15**(2), 021316.

73 I. Mondal, S. Raj, P. Roy and R. Poddar, Silver nanoparticles (AgNPs) as a contrast agent for imaging of animal tissue using swept-source optical coherence tomography (SSOCT), *Laser Phys.*, 2017, **28**(1), 015601.

74 S. A. Brennan, C. Ni Fhoghlu, B. M. Devitt, F. J. O'Mahony, D. Brabazon and A. Walsh, Silver nanoparticles and their orthopaedic applications, *Bone Joint J.*, 2015, **97**(5), 582–589.

75 F. Benyettou, R. Rezgui, F. Ravaux, T. Jaber, K. Blumer, M. Jouiad, L. Motte, J. C. Olsen, C. Platas-Iglesias, M. Magzoub and A. Trabolsi, Synthesis of silver nanoparticles for the dual delivery of doxorubicin and alendronate to cancer cells, *J. Mater. Chem. B*, 2015, **3**(36), 7237–7245.

76 Z. Hussain, M. A. S. Abourehab, S. Khan and H. E. Thu, Chapter 9 – Silver nanoparticles: a promising nanoplatform for targeted delivery of therapeutics and optimized therapeutic efficacy, in *Metal Nanoparticles for Drug Delivery and Diagnostic Applications*, ed. Shah M. R., Imran M. and Ullah S., Elsevier, 2020, pp. 141–173.

77 S. H. Lee and B.-H. Jun, Silver Nanoparticles: Synthesis and Application for Nanomedicine, *Int. J. Mol. Sci.*, 2019, **20**(4), 865.

78 T. Huang and X.-H. Nancy Xu, Synthesis and Characterization of Tunable Rainbow Colored Colloidal Silver Nanoparticles Using Single-Nanoparticle Plasmonic Microscopy and Spectroscopy, *J. Mater. Chem.*, 2010, **20**(44), 9867–9876.

79 A. P. Stevenson, D. Blanco Bea, S. Civit, S. Antoranz Contera, A. Iglesias Cerveto and S. Trigueros, Three strategies to stabilise nearly monodispersed silver nanoparticles in aqueous solution, *Nanoscale Res. Lett.*, 2012, **7**(1), 151.

80 C. Liu, W. Leng and P. J. Vikesland, Controlled Evaluation of the Impacts of Surface Coatings on Silver Nanoparticle Dissolution Rates, *Environ. Sci. Technol.*, 2018, **52**(5), 2726–2734.

81 R. G. Sanedrin, L. Huang, J. W. Jang, J. Kakkassery and C. A. Mirkin, Polyethylene glycol as a novel resist and sacrificial material for generating positive and negative nanostructures, *Small*, 2008, **4**(7), 920–924.

82 C. Luo, Y. Zhang, X. Zeng, Y. Zeng and Y. Wang, The role of poly(ethylene glycol) in the formation of silver nanoparticles, *J. Colloid Interface Sci.*, 2005, **288**(2), 444–448.

83 A. Shkilnyy, M. Souce, P. Dubois, F. Warmont, M. L. Saboungi and I. Chourpa, Poly(ethylene glycol)-stabilized silver nanoparticles for bioanalytical applications of SERS spectroscopy, *Analyst*, 2009, **134**(9), 1868–1872.

84 J. A. Bonventre, J. B. Pryor, B. J. Harper and S. L. Harper, The impact of aminated surface ligands and silica shells on the stability, uptake, and toxicity of engineered silver nanoparticles, *J. Nanopart. Res.*, 2014, **16**(12), 2761.

85 R. Karunamuni, P. C. Naha, K. C. Lau, A. Al-Zaki, A. V. Popov, E. J. Delikatny, A. Tsourkas, D. P. Cormode and A. D. Maidment, Development of silica-encapsulated silver nanoparticles as contrast agents intended for dual-energy mammography, *European Radiology*, 2016, **26**(9), 3301–3309.

86 P. C. Naha, K. C. Lau, J. C. Hsu, M. Hajfathalian, S. Mian, P. Chhour, L. Uppuluri, E. S. McDonald, A. D. A. Maidment and D. P. Cormode, Gold silver alloy nanoparticles (GSAN): an imaging probe for breast cancer screening with dual-energy mammography or computed tomography, *Nanoscale*, 2016, **8**(28), 13740–13754.

87 C. W. Moon, J. Park, S.-P. Hong, W. Sohn, D. M. Andoshe, M. Shokouhimehr and H. W. Jang, Decoration of metal oxide surface with {111} form Au nanoparticles using PEGylation, *RSC Adv.*, 2018, **8**(33), 18442–18450.

88 M. R. Mackiewicz, H. L. Hodges and S. M. Reed, C-Reactive Protein Induced Rearrangement of Phosphatidylcholine on Nanoparticle Mimics of Lipoprotein Particles, *J. Phys. Chem. B*, 2010, **114**(16), 5556–5562.

89 S. Sitaula, M. R. Mackiewicz and S. M. Reed, Gold nanoparticles become stable to cyanide etch when coated with hybrid lipid bilayers, *Chem. Commun.*, 2008, (26), 3013–3015.

90 M. S. Wang, R. E. Messersmith and S. M. Reed, Membrane curvature recognition by C-reactive protein using lipoprotein mimics, *Soft Matter*, 2012, **8**(30), 7909–7918.

91 C. J. Orendorff and C. J. Murphy, Quantitation of Metal Content in the Silver-Assisted Growth of Gold Nanorods, *J. Phys. Chem. B*, 2006, **110**(9), 3990–3994.

92 S.-C. Wei, P.-H. Hsu, Y.-F. Lee, Y.-W. Lin and C.-C. Huang, Selective Detection of Iodide and Cyanide Anions Using Gold-Nanoparticle-Based Fluorescent Probes, *ACS Appl. Mater. Interfaces*, 2012, **4**(5), 2652–2658.

93 X. Liu, M. Yu, H. Kim, M. Mameli and F. Stellacci, Determination of monolayer-protected gold nanoparticle ligand–shell morphology using NMR, *Nat. Commun.*, 2012, **3**, 1182.

94 T. Zhu, K. Vasilev, M. Kreiter, S. Mittler and W. Knoll, Surface Modification of Citrate-Reduced Colloidal Gold Nanoparticles with 2-Mercaptosuccinic Acid, *Langmuir*, 2003, **19**(22), 9518–9525.

95 G. S. Métraux and C. A. Mirkin, Rapid Thermal Synthesis of Silver Nanoprisms with Chemically Tailorable Thickness, *Adv. Mater.*, 2005, **17**(4), 412–415.

96 S. Chen, Z. Fan and D. L. Carroll, Silver Nanodisks: Synthesis, Characterization, and Self-Assembly, *J. Phys. Chem. B*, 2002, **106**(42), 10777–10781.

97 A. Henglein and M. Giersig, Formation of Colloidal Silver Nanoparticles: Capping Action of Citrate, *J. Phys. Chem. B*, 1999, **103**(44), 9533–9539.

98 A. C. Templeton, M. J. Hostetler, C. T. Kraft and R. W. Murray, Reactivity of Monolayer-Protected Gold Cluster Molecules: Steric Effects, *J. Am. Chem. Soc.*, 1998, **120**(8), 1906–1911.

99 S. Hajizadeh, K. Farhadi, M. Forough and R. E. Sabzi, Silver nanoparticles as a cyanide colorimetric sensor in aqueous media, *Anal. Methods*, 2011, **3**(11), 2599–2603.

100 C.-Y. Ke, T.-H. Chen, L.-C. Lu and W.-L. Tseng, Understanding thiol-induced etching of luminescent gold nanoclusters, *RSC Adv.*, 2014, **4**(50), 26050–26056.

101 R. Behra, L. Sigg, M. J. D. Clift, F. Herzog, M. Minghetti, B. Johnston, A. Petri-Fink and B. Rothen-Rutishauser, Bioavailability of silver nanoparticles and ions: from a chemical and biochemical perspective, *J. R. Soc., Interface*, 2013, **10**(87), 20130396.

102 K. A. Huynh and K. L. Chen, Aggregation kinetics of citrate and polyvinylpyrrolidone coated silver nanoparticles in monovalent and divalent electrolyte solutions, *Environ. Sci. Technol.*, 2011, **45**(13), 5564–5571.

103 J. Liu and R. H. Hurt, Ion Release Kinetics and Particle Persistence in Aqueous Nano-Silver Colloids, *Environ. Sci. Technol.*, 2010, **44**(6), 2169–2175.

104 A. Bradford, R. D. Handy, J. W. Readman, A. Atfield and M. Mühling, Impact of Silver Nanoparticle Contamination on the Genetic Diversity of Natural Bacterial Assemblages in Estuarine Sediments, *Environ. Sci. Technol.*, 2009, **43**(12), 4530–4536.

105 J. Fabrega, S. R. Fawcett, J. C. Renshaw and J. R. Lead, Silver Nanoparticle Impact on Bacterial Growth: Effect of pH, Concentration, and Organic Matter, *Environ. Sci. Technol.*, 2009, **43**(19), 7285–7290.

106 J. Jiang, G. Oberdörster and P. Biswas, Characterization of size, surface charge, and agglomeration state of nanoparticle dispersions for toxicological studies, *J. Nanopart. Res.*, 2009, **11**(1), 77–89.

107 I. Sondi and B. Salopek-Sondi, Silver nanoparticles as antimicrobial agent: a case study on E. coli as a model for Gram-negative bacteria, *J. Colloid Interface Sci.*, 2004, **275**(1), 177–182.

108 A. M. El Badawy, T. P. Luxton, R. G. Silva, K. G. Scheckel, M. T. Suidan and T. M. Tolaymat, Impact of environmental conditions (pH, ionic strength, and electrolyte type) on the surface charge and aggregation of silver nanoparticles suspensions, *Environ. Sci. Technol.*, 2010, **44**(4), 1260–1266.

109 F. Piccapietra, L. Sigg and R. Behra, Colloidal stability of carbonate-coated silver nanoparticles in synthetic and natural freshwater, *Environ. Sci. Technol.*, 2012, **46**(2), 818–825.

110 C. Levard, S. Mitra, T. Yang, A. D. Jew, A. R. Badireddy, G. V. Lowry and G. E. Brown, Effect of Chloride on the Dissolution Rate of Silver Nanoparticles and Toxicity to E. coli, *Environ. Sci. Technol.*, 2013, **47**(11), 5738–5745.

111 J. Liu and R. H. Hurt, Ion release kinetics and particle persistence in aqueous nano-silver colloids, *Environ. Sci. Technol.*, 2010, **44**(6), 2169–2175.

112 C. Greulich, J. Diendorf, T. Simon, G. Eggeler, M. Epple and M. Koller, Uptake and intracellular distribution of silver nanoparticles in human mesenchymal stem cells, *Acta Biomater.*, 2011, **7**(1), 347–354.

113 K. Loza, J. Diendorf, C. Sengstock, L. Ruiz-Gonzalez, J. M. Gonzalez-Calbet, M. Vallet-Regi, M. Köller and M. Epple, The dissolution and biological effects of silver nanoparticles in biological media, *J. Mater. Chem. B*, 2014, **2**(12), 1634–1643.

114 A. M. Bakke, C. Glover and A. Krogdahl, Feeding, digestion and absorption of nutrients, in *The multifunctional gut of fish*, ed. M. Grosell, A. P. Farrell and C. J. Brauner, Academic Press, London, UK, 2011, pp. 57–110.

115 A. P. Gondikas, A. Morris, B. C. Reinsch, S. M. Marinakos, G. V. Lowry and H. Hsu-Kim, Cysteine-Induced Modifications of Zero-valent Silver Nanomaterials: Implications for Particle Surface Chemistry, Aggregation, Dissolution, and Silver Speciation, *Environ. Sci. Technol.*, 2012, **46**(13), 7037–7045.

116 R. A. Bell and J. R. Kramer, Structural chemistry and geochemistry of silver-sulfur compounds: Critical review, *Environ. Toxicol. Chem.*, 1999, **18**(1), 9–22.

117 J. Liu, D. A. Sonshine, S. Shervani and R. H. Hurt, Controlled Release of Biologically Active Silver from Nanosilver Surfaces, *ACS Nano*, 2010, **4**(11), 6903–6913.

118 Z.-M. Xiu, J. Ma and P. J. J. Alvarez, Differential Effect of Common Ligands and Molecular Oxygen on Antimicrobial Activity of Silver Nanoparticles versus Silver Ions, *Environ. Sci. Technol.*, 2011, **45**(20), 9003–9008.

119 C. Levard, B. C. Reinsch, F. M. Michel, C. Oumahi, G. V. Lowry and G. E. Brown, Sulfidation processes of PVP-coated silver nanoparticles in aqueous solution: impact on dissolution rate, *Environ. Sci. Technol.*, 2011, **45**(12), 5260–5266.

120 A. Melcrová, S. Pokorna, S. Pullanchery, M. Kohagen, P. Jurkiewicz, M. Hof, P. Jungwirth, P. S. Cremer and L. Cwiklik, The complex nature of calcium cation interactions with phospholipid bilayers, *Sci. Rep.*, 2016, **6**, 38035.

121 D. Papahadjopoulos, W. J. Vail, K. Jacobson and G. Poste, Cochleate lipid cylinders: formation by fusion of unilamellar lipid vesicles, *Biochim. Biophys. Acta*, 1975, **394**(3), 483–491.

122 T. Ito and S. Onishi, Ca2+-induced lateral phase separations in phosphatidic acid-phosphatidylcholine membranes, *Biochim. Biophys. Acta*, 1974, **352**(1), 29–37.

123 R. Dluhy, D. G. Cameron, H. H. Mantsch and R. Mendelsohn, Fourier transform infrared spectroscopic studies of the effect of calcium ions on phosphatidylserine, *Biochemistry*, 1983, **22**(26), 6318–6325.

124 K. Naga, N. H. Rich and K. M. W. Keough, Interaction between dipalmitoylphosphatidylglycerol and phosphatidylcholine and calcium, *Thin Solid Films*, 1994, **244**(1), 841–844.

125 L. Zhang, X. Li, R. He, L. Wu, L. Zhang and J. Zeng, Chloride-induced shape transformation of silver nanoparticles in a water environment, *Environ. Pollut.*, 2015, **204**, 145–151.